



A covalent organic framework onion structure

Qi Zheng^{1,2}, Xinle Li^{3,#}, Qiubo Zhang¹, Daewon Lee^{1,4}, Haiyan Mao⁵,
Chongqing Yang³, Karen C. Bustillo³, Jeffrey A. Reimer^{1,5}, Yi Liu³,
Jinyang Jiang², Haimei Zheng^{1,4,*}

¹ Materials Sciences Division, Lawrence Berkeley National Laboratory, Berkeley, CA 94720, United States

² School of Materials Science and Engineering, Southeast University, Nanjing 211189, PR China

³ The Molecular Foundry, Lawrence Berkeley National Laboratory, Berkeley, CA 94720, United States

⁴ Department of Materials Science and Engineering, University of California, Berkeley, CA 94720, United States

⁵ Department of Chemical and Biomolecular Engineering, University of California, Berkeley, CA 94720, United States

Achieving hierarchical nanomaterials from a bottom-up approach remains challenging. Here, we report a closed-cage, onion nanostructure of covalent organic framework (COF) obtained through a low-temperature solvothermal synthesis. Atomic resolution transmission electron microscopy revealed the atomic arrangement in this COF onion, in which rich nitrogen was uniformly embedded in the periodic porous graphitic framework. The COF onion structure displayed graphitic features at a 0.33 nm interlayer spacing with Van der Waals interactions predominated between the layers. The onion layers exhibited significant heterogeneity in layer stacking by adopting a combination of different stacking modes. Defects were also found, such as five- or seven-member rings deviating from the perfect hexagonal lattice. These geometrical defects resulted in curving the 2D layers, which may have promoted the formation of onion nanostructures through a layer-by-layer attachment. We constructed a corresponding model that predicts COF onion properties. This novel onion exhibited a bandgap value of 2.56 eV, resembling other carbon-based nanomaterials, suggesting potential applications in sensors, photocatalysts, and nanoelectronics.

Keywords: C–N onion nanostructure; Covalent organic framework (COF); Atomic bonding; Stacking modes; Transmission electron microscopy (TEM)

Introduction

Although graphite, with two-dimensional layers stacking together, is one of the stable forms of carbon under ambient conditions, at the nanometer scale, it forms zero-dimensional structures, such as graphene quantum dots [1,2], and fullerenes [3–5]. Such dimension reduction brings new opportunities to access

unusual material properties through the control of nanostructures [6,7]. For instance, carbon onion structures have incurred great interest in the formation mechanism and structure–property relationships. This virtue is not limited to carbon, and, in recent years, onion structures have been made from numerous compounds with layered two-dimensional nanostructures [8,9]. Onion nanostructures can exist in many 2D layers, such as graphene [22], BN [23], MoS₂ [24], WS₂ [25], and Cs₂O [26]. However, most of these syntheses involve high-temperature or high-pressure processes, such as flaming, solar ablation, or deto-

* Corresponding author.

E-mail address: Zheng, H. (hmzheng@lbl.gov)

Current address: Department of Chemistry, Clark Atlanta University, Atlanta, GA 30314, United States.

nation. Controllable fabrication of onion nanostructures in a mild condition is of considerable scientific interest and has not been achieved previously.

Covalent organic frameworks (COFs) are crystalline porous polymers integrating organic units into extended periodic networks with atomic precision [10]. 2D COFs are obtained by covalently assembling the organic monomeric units in the desired geometry [11]. Due to the hybridized states (sp , sp^2 , sp^3) of carbon [12–14] with diverse bonding in the COF structure, complex nanostructures, such as spheres [15], belts [16], or microtubes [17], have been achieved. These complex nanostructures possess properties that differ significantly from their bulk counterparts [18–21]. Considering the exceedingly designable architecture and versatile applications of COFs, the controllable synthesis of COF-based nanostructures is of prime importance. COF onion structures, made from metal-free, purely organic-based 2D frameworks, may incur new insight into the formation mechanism and the material properties. The synthesis and characterization of such COF onions are, however, unprecedented and need to be explored.

In this work, a novel carbon–nitrogen (C–N) COF onion was obtained through a facile low-temperature solvothermal process. We identified its atomic structure and deciphered its layer stacking features via transmission electron microscopy (TEM). Advanced chemical mapping coupled with electron energy-loss spectroscopy (EELS) was employed to determine the elemental and atomic bonding characters. The onion structure is highly nitrogenous with distinct graphitic features in a combinational stacking mode. The novel C–N COF onion presents a bandgap at ~ 2.6 eV owing to its intrinsic sp^2 hybridized conjugated skeletons. We expect broad applications of these COF onions, such as in sensors, photocatalysts, and nanoelectronics.

Results and discussions

Identification of a novel C–N COF onion

We previously synthesized a 2D pyrazine-fused porous graphitic framework through a solvothermal process at 120 °C [27]. The reversible condensation of 1,2,4,5-benzenetetramine (BTA) tetrahydrochloride and hexaketocyclohexane (HKH) octahydrate under basic conditions produced highly crystalline graphitic layers. Some of the products can exhibit the onion morphology through a possible 2D transformation. By selecting the suitable solvent (N-Methyl-2-Pyrrolidone, NMP) coupled with optimal centrifuge procedures, we successfully separated the onion phases and discovered a novel C–N COF onion, made from metal-free, purely organic-based 2D frameworks (Fig. 1a).

Similar to traditional carbon onions, our COF onion consists of concentric shells in a polyhedral shape (Fig. 1b). In Fig. 1c, these 2D layers possess highly fused aromatic backbones, periodic nanopores (~ 1.2 nm), and π -stacking columns with an interlayer stacking distance of approximately 0.33 nm. We found that the individual COF onion particle can possess a size up to 10 nm (Fig. 1d) with a central void. Different porosity may be attained by adjusting the void size. There is a tendency for the shell thickness to decrease with a larger void inside (Fig. 1e). For example, the shell is 9 nm when the central void is 3.2 nm, compared with only a 4 nm shell grown on a 5.5 nm void. This is presumably governed by the surface energy [28].

Although the onion particles display different features, the measured d spacing between two adjacent layers remains the same as 0.33 nm (Fig. 1f, using the intensity profiles), which agrees with the interlayer distance of bulk COFs (Fig. S1).

Elemental and bonding structure of C–N COF onions

Highly concentrated COF onions were achieved through an optimal centrifuge procedure and were illustrated in Fig. 2a (see method for details). We observed that the onions display graphitic layers at a 0.33 nm spacing indicated by the inserted FFT pattern. The surface electrostatic potential is relatively high considering the nanosize effect of onion particles, which can induce the aggregation of COF onions. Similar clustering phenomena have been reported in other carbon-based materials such as nanodiamonds [29]. We performed quantitative analysis on the COF onion aggregates (Fig. 2b) and found that the particles exhibit an average size of 5.7 nm, including a 1.7 nm graphitic shell. Geometrically, the onions are primarily convex with a polydispersity from 0.4 to 0.8 in the circularity. The average aspect ratio is estimated at 1.8, representing an oval shape of onion aggregates.

According to the energy dispersive spectroscopy (EDS) mapping in Fig. 2c, both carbon and nitrogen elements are uniformly distributed in the COF onions. A rich nitrogen composition of up to ~ 25 % (At) was detected (Fig. S2). As each BTA molecule contains 4 nitrogen atoms, the COF onion structure shares the formula of $(C_5N_2H_1)_n$ if it is fully decorated with nitrogen. This is also consistent with the results from the full EELS spectrum in Fig. 2d.

We applied electron energy-loss spectroscopy (EELS) to study the interatomic bonding of the COF onions. Carbon and nitrogen are evaluated as the main chemical composition in the COF onions (Fig. 2d). A sharp N K-edge demonstrated the high concentration of nitrogen elements in the COF onion. The pronounced peak at ~ 20 eV in the low loss spectrum (Fig. 2e) was assigned to the $\pi + \sigma$ plasmon owing to the collective oscillation of π and σ valence electrons [30]. Another peak at 6.5 eV is the sign of π plasmon from the sp^2 bonding in the COF onion, which is common in graphite or other sp^2 -carbon-based materials [31]. We further examined near-edge fine structures between carbon–nitrogen linkages. In detail, the peak at 286.8 eV represents $1s \rightarrow \pi^*$ transitions of sp^2 carbon while the main edge at ~ 297 eV is due to $1s \rightarrow \sigma^*$ transitions from sp^3 bonds [32]. It is reasonable that sp^3 carbon single bonds remain in COFs due to some structural defects [33]. Similarly, the nitrogen peak at 396.8 eV is ascribed to $1s \rightarrow \pi^*$ transition [34]. This strong nitrogen π^* peak indicated significant nitrogen in sp^2 -bonded aromatic rings in the form of a pyridine structure [35,36]. The findings in EELS confirm that carbon and nitrogen in COF onions are dominated in the characteristic sp^2 bonding, which is consistent with the structure shown in Fig. 1.

The Fourier transform infrared (FTIR) spectrum (Fig. 2f) shows the characteristic pyrazine stretching bands at 1238 cm^{-1} [37]. Different from the amorphous nitrogen-doped systems [38], we have achieved a unique nitrogenous onion structure with ordered atomic arrangements. ^{13}C cross-polarization magic angle spinning (^{13}C -CP/MAS) NMR spectroscopy (Fig. 2g) further confirmed the formation of pyrazine linkages. The NMR spectrum

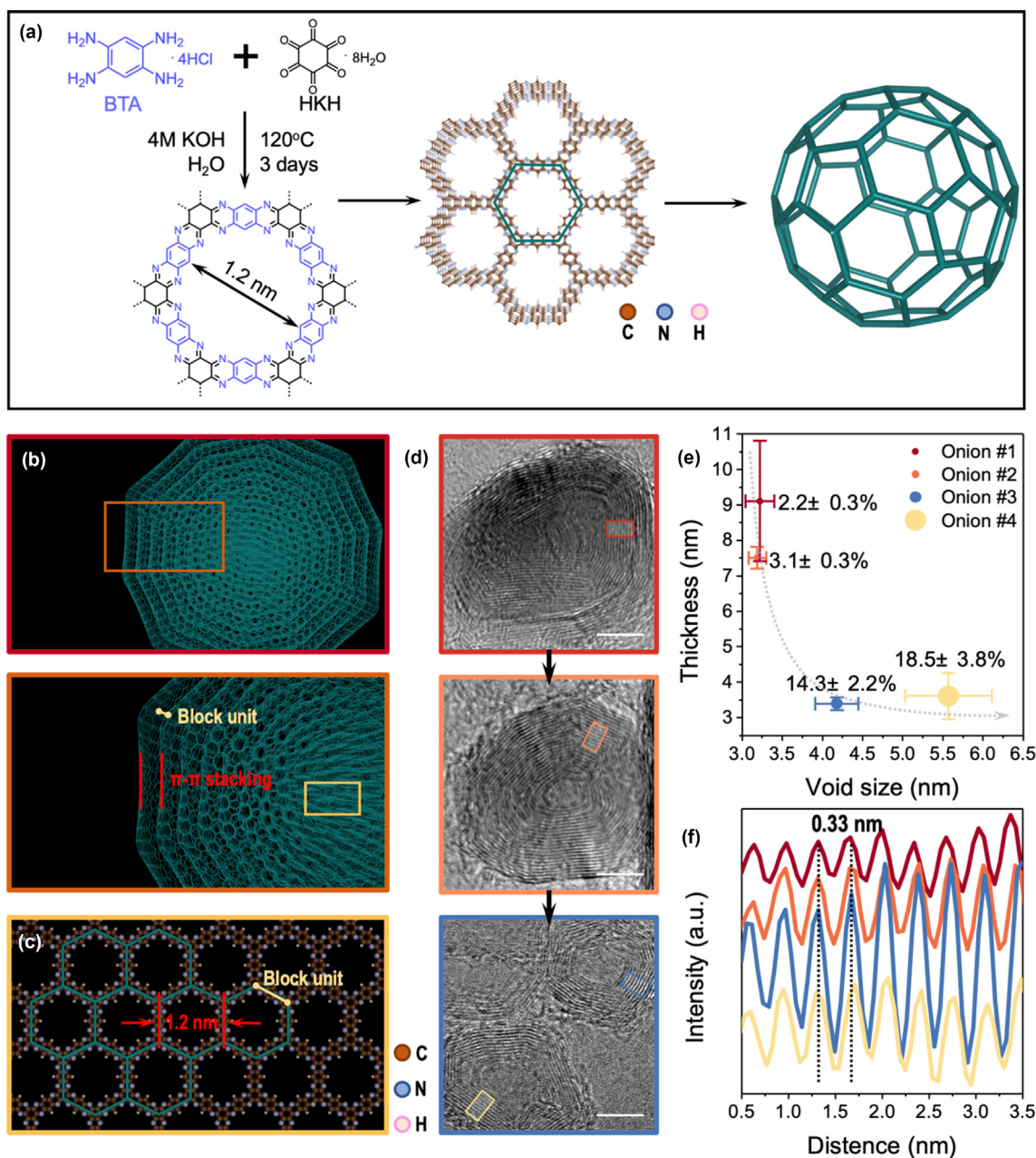


FIGURE 1

Discovery of a COF onion. (a) A schematic of the synthesis method. Condensation between 1,2,4,5-benzenetetramine tetrahydrochloride (BTA) and hexaketocyclohexane octahydrate (HKH) under a basic hydrothermal environment leads to the formation of a COF onion. Note that potassium hydroxide solution acts as the catalyst. (b) Illustration of a COF onion at different scales. Concentric shells with an interlayer spacing of 0.33 nm can be observed. (c) The COF onion is composed of aza-fused aromatic backbones with well-arranged 1.2 nm pores. (d) High resolution transmission electron microscopy (HRTEM) images of four representative COF onions. The onion exhibits a “void-shell” structure with graphite-like shells. Scale bars, 5 nm. (e) The relation between the void size and shell thickness in different onions (the color is consistent with the border color in (d)). The porosity (the ratio between the void and the whole onion, calculated by projected area) of the onion is labeled along with data points. The error bar is estimated by multiple calculations. (f) The distance between the two layers is calculated at 0.33 nm based on the gray value intensity profiles in the highlighted regions in (d).

showed resonances signaled at 108, 134, and 142 ppm, which could be assigned to the pyrazine carbon atoms adjacent to the nitrogen atoms, carbon atoms of the hexaazatrinaphthalene nodes on vertices, and the unsubstituted carbon atoms of the phenyl edge, respectively [39]. Both NMR and FTIR validated the conjugated sp² pyrazine structure in COF onions.

Stacking modes of C–N COF onion layers

In Fig. 3a, each graphitic layer in the onion was traced and color-coded by its local curvature. The result indicates that the onion is a polyhedron, with its terraces possessing higher curvature values. More specifically, the COF onion particle shows a fivefold symmetry. It exhibits some inherent characters: the region in

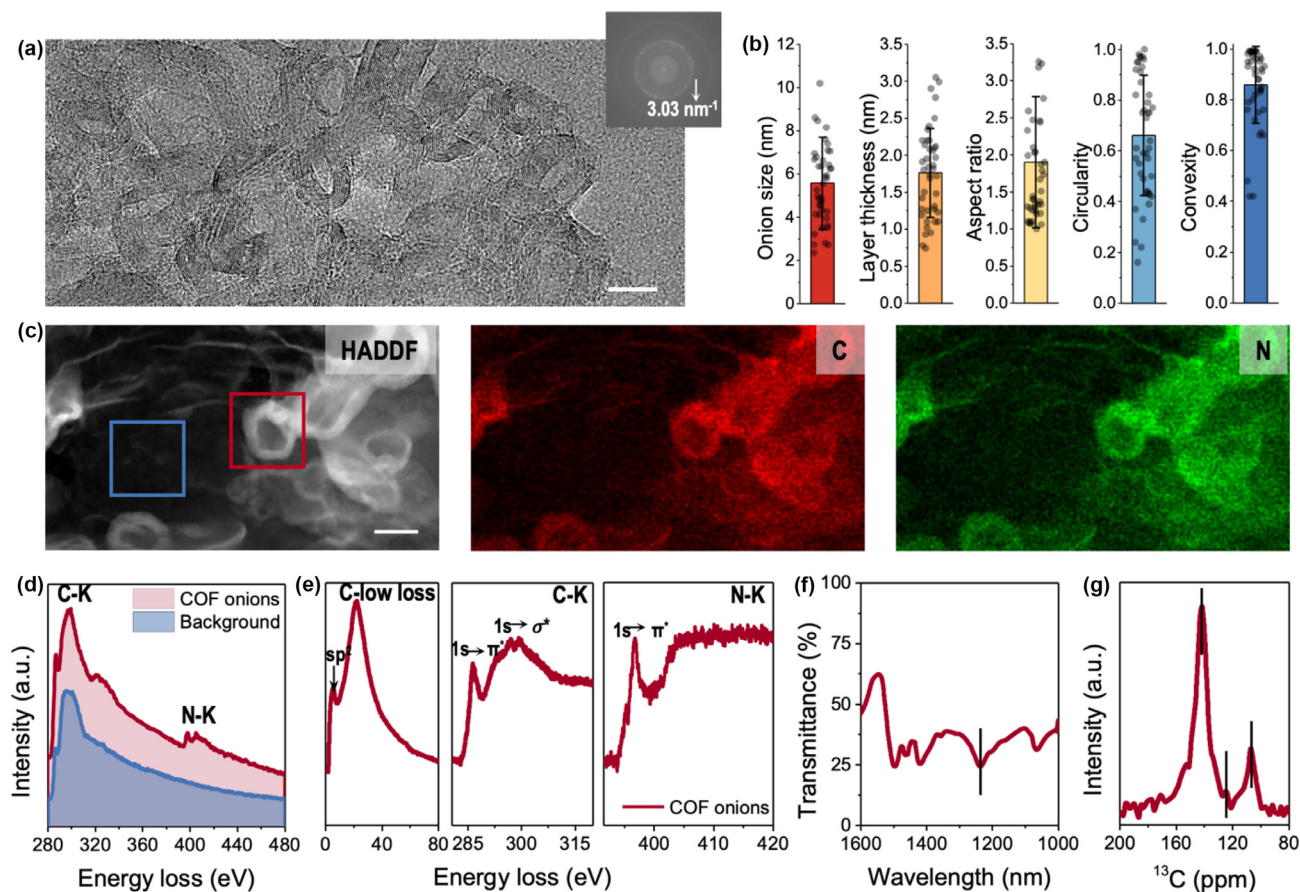


FIGURE 2

The structural and elemental information of COF onions. (a) COF onions with an interlayer spacing of 0.33 nm. Scale bar, 10 nm. Inserted is its corresponding FFT pattern. (b) Structure parameters of COF onions, including size, shell thickness, aspect ratio, circularity, and convexity, were calculated from (a). The entire frame TEM image can be found in Supporting Information, as well as definitions of the parameters and calculation formulas. Each dot represents one measurement, and the error bar is the standard deviation from the sampling. (c) Elemental mapping of COF onions. STEM-HAADF image and EDS maps of carbon (red) and nitrogen (green). Two regions with or without onions are highlighted in boxes for further EELS measurements in (d). Scale bar, 50 nm. (d) EELS spectra of COF onions and carbon film background. (e) Low loss spectrum of C with a sp^2 peak distinguishable. The zero-loss line and the double scattering contributions are subtracted from the data. Near-edge structure of the C K-edge and N K-edge after individual subtraction of an inverse-power-law background. (f) The Fourier transform infrared (FTIR) spectrum of COF onions. The peak at 1238 cm^{-1} represents $-C=N-$ linkages. (g) Solid-state ^{13}C cross-polarization magic angle spinning (^{13}C CP-MAS) NMR chemical shift spectrum of COF onions. The states of carbons can be classified into the pyrazine carbons adjacent to the nitrogen atoms (108 ppm), and carbons of the hexaazatriphthalene (HATN) cores on vertices (134 ppm), and the unsubstituted carbons of the phenyl edge (142 ppm).

the inner shell at a high curvature value may result in the outer shell region becoming much curled accordingly. The evidence manifests the possible mechanism of onion growth through a layer-by-layer attachment. The onion structure was also confirmed by the simulated TEM image in Fig. 3b (also see Fig. S3). The further tomographic analysis supports a real 3D onion structure by a series of tilting (Fig. S4).

The radial intensity profile in Fig. 3c exhibits three prominent diffraction peaks. The broad peak at 0.12 \AA^{-1} can be assigned to the (100) facet, representing the structure facet with hexagonally arranged pores of 1.2 nm. According to structural simulations with different stacking configurations, the (001) at 0.3 \AA^{-1} corresponds to the π - π stacking of onion layers [40]. Moreover, the peak at the spacing of 2.1 \AA is consistent with the size of the aromatic pyrazine ring [27]. In Fig. 3d, the local interlayer spacing of 2D layers was captured (see more details in Supporting Information). Van der Waals interactions are predominated between the onion layers, and we found significant heterogeneity in the

stacking. As expected, the surface layers share a larger interlayer spacing up to 0.5 \AA , attributed to the surface energy-induced reconstruction [41]. Defects or dislocations can also cause different stacking configurations. For example, some local regions such as the onion corners, boundaries, and terraces (see arrows in Fig. 3d) also exhibit localized expansion. A bimodal distribution of interlayer spacing is noted in Fig. 3e. The first peak at 0.33 nm is the normal stacking, while the peak at 0.37 nm is caused by the stacking distortion from the surfaces and boundaries [42]. The layer stacking mode is combinational. Here, we postulate a model including AA, AB, and SP (saddle point) stacking considering the large variety of interlayer spacing obtained. The heterogeneous stacking of layers can be the inherent mechanism for forming onion structure through flexible conformation since abundant stacking faults can be commonly distinguished in the COF onions (Fig. 3f).

Traditional onion nanostructures, including graphene onions, and MoS_2 onions are generated using high-

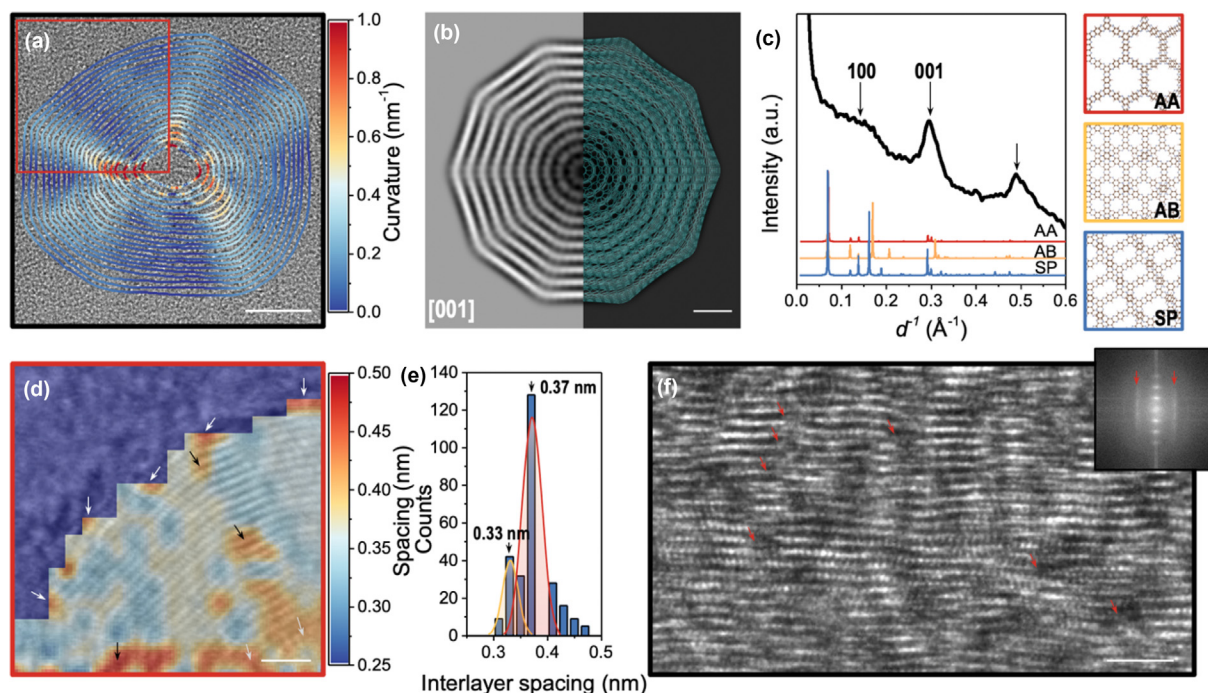


FIGURE 3

Layer stacking modes in COF onion. (a) Map of the graphitic layers in the onion structure color-coded by the local curvature. Scale bar, 5 nm. The original TEM image and detailed image analysis method can be found in Supporting Information. (b) Multi-slice TEM simulation on a polyhedron onion, observed from the [001] perspective. Scale bar, 1 nm. (c) Radial intensity profile of COF onion derived from the diffraction. Some peaks can be assigned to certain facets according to diffraction simulations on different stacking modes of COF layers. (d) Mapping the interlayer spacing of the COF onion based on the magnified region in (a). Scale bar, 2 nm. The spacing is calculated by the partitioned FFT analysis based on a 10x10 proportion step with an overlap of 10 pixels. More details can be found in Supporting Information. (e) Distribution of the interlayer spacing, fitted using Gaussian functions. (f) Heterogeneity of layer stacking in the onion structure. Defects and stacking faults are highlighted by arrows. Scale bar, 2 nm. The inserted is the corresponding FFT pattern, showing streaking due to stacking faults.

temperature/ high-pressure processes. Such methods provide high-intensity shockwaves that cause local heterogeneity in the system, which can lead to heterogeneous nucleation and growth. We proposed that the formation of COF onions is also controlled by the nanoscale heterogeneity and fluctuations in the basic aqueous solution (Fig. 4) [43].

In detail, a homogenous solution can be obtained initially upon the dissolution of BTA and HKH precursors in water. Then, clusters containing oligomers appear with some ordering features. Subsequently, discontinuous graphitic COF layers can be observed from the supersaturated aqueous solution, and they attached together to form an onion structure (Fig. 4a). Because defects occur during the condensation, these graphitic layers tend to fold to minimize surface energy according to our molecular dynamics simulations (Fig. 4b). For example, some of the COF flocs may contain five- or seven-member macrocyclic rings that are prone to be stabilized as curved structures after a sufficient structural relaxation. In detail, we observed the whole folding process of defected COF layers which are originally planar. It was captured that the bending initiates at the five-member rings and thus forms cone-like structures. These COF cones can be the intermediates in the formation of COF onions. Such a process can be super-fast within 2 ns to reach the equilibrium state. Note that different defects can alter the shape of onions from spherical to oval ones, leading to the final onion products of varying sizes and circularities.

Interestingly, defects can promote the folding of layers to achieve a higher curvature value, and accelerate the zip-up process, which means the more defects in the COF structure, the higher structural curvature may be achieved. Consequently, the COF onions may grow layer by layer to form the nested layered nanostructure (Fig. 4c). Firstly, the optimal interlayer spacing at 0.33 nm can be readily attained followed by a planar structural adjustment, for example, through layer sliding, to accomplish the complex interlayer stacking as demonstrated in Fig. 3.

We proposed a perfect COF onion belonging to the icosahedral family (Fig. S5, also see detailed construction methods in Fig. S6). Note that different onion models can be constructed based on the geometry criterion [44]. Our COF onion model consists of 12 pentagonal rings and hexagonal ones in a certain number, which can be calculated using Euler's theorem. The hexagonal rings in the center are in a planar configuration, while the pentagonal rings at vertices bend in an inward longitudinal curvature. These pentagons can provoke the curving of the COF nucleus into a bowl-shaped structure and thus zip up its open edges, ending up with a closed onion structure during the crystallization process [45].

Optical properties of COF onions

Furthermore, we investigated the optical properties of COF onions for their potential applications. Direct UV-vis measurement reflects a broad absorption (Fig. 5a) with an optical band-

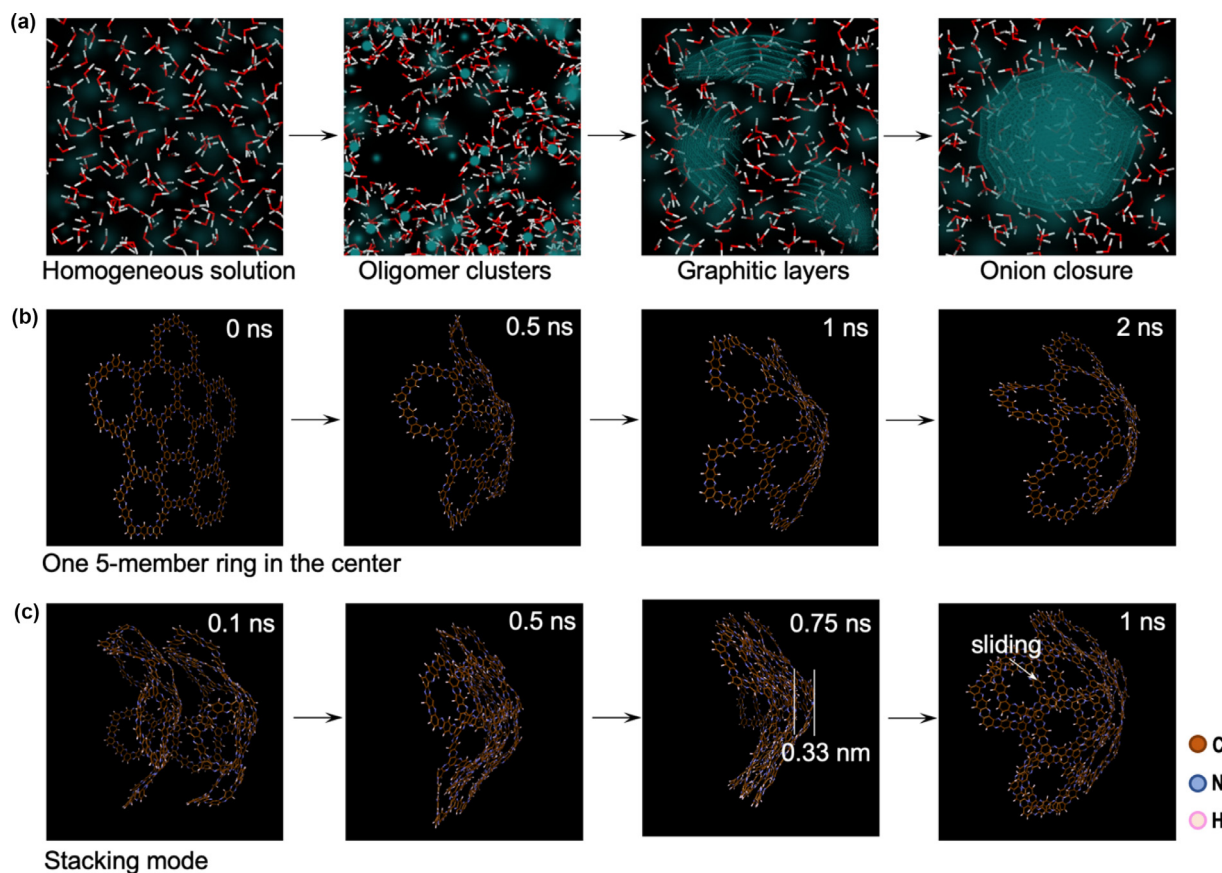


FIGURE 4

Proposed formation pathways of COF onions in solution. (a) Schematic illustration of the growth mechanism of COF onions, including the nucleation of oligomer clusters in the supersaturated aqueous solution; the formation of the graphitic layers; thickening of the onion fragments, and the closure of onion particles. (b) Molecular dynamics simulations on COF fragments with a five-member ring defect. The initial folding occurs at the defect center. (c) Molecular dynamics simulations on the stacking process of two COF layers. The configurations at different relaxation time are highlighted.

gap of 2.56 eV. Some parameters such as the defect ratio, and the curvature of the COF layers, were explored based on theoretical calculations. After constructing a series of COF single layer models with different defects, we performed quantum chemistry calculations to determine their optical bandgaps using the HOMO-LUMO gap from the single point calculation. In Fig. 5b, the bandgap increases at a higher defect ratio. The perfect COF layer features a fully annulated aromatic skeleton, which is a sp^2 conjugated structure with a dominantly π character. It possesses a low optical bandgap at 1.38 eV (see the bulk layered COF in Fig. 5d). As the defects are introduced into the structure, such as five- or seven-member rings, the perfect hexagonal lattice can be significantly distorted. More π -bonding transits into σ character due to the change from sp^2 to sp^3 hybridization, which is consistent with the findings in our EELS analysis that some sp^3 bonding characters were distinguished (Fig. 2). Therefore, the bandgap increases with more defects present in the framework. Accordingly, as the defects trigger the curvature of a flat COF layer to form an oval structure (i.e., oval structure shares a larger curvature than the flat COF layer), the bandgap also rises when the structure is at a higher curvature value (Fig. 5c). This agrees

with the observations in the polyaromatic hydrocarbons [46,47]. Note that the morphology of COF may be different even using the same starting chemicals under different experimental conditions; we found the synthesized bulk COF layers exhibit a lower bandgap at 1.38 eV. This is reasonable concerning the defect and curvature effects aforementioned. The findings also indicate the opportunities to tune the bandgap of COF onions through defect engineering inspired by the techniques used in graphene nanoribbons [48–50]. We compared the optical bandgap of COF onion with other carbon-based materials (Fig. 5d). Its value is similar to fullerenes [51]. Although it may not be fluorescent, some methods like selective addition, by dividing its π -conjugated system into small parts, can be promising to enhance its fluorescent properties [52].

Meanwhile, the COF onion is surprisingly stable, and it deforms at a high yield strength without crack propagation from the fracture according to our molecular dynamics simulation (Fig. S7). The exceptional plasticity of this COF onion could be useful in nanoscopic pressure cells [56] or other flexible electronics [57], which significantly extends the applications of carbon-family materials.

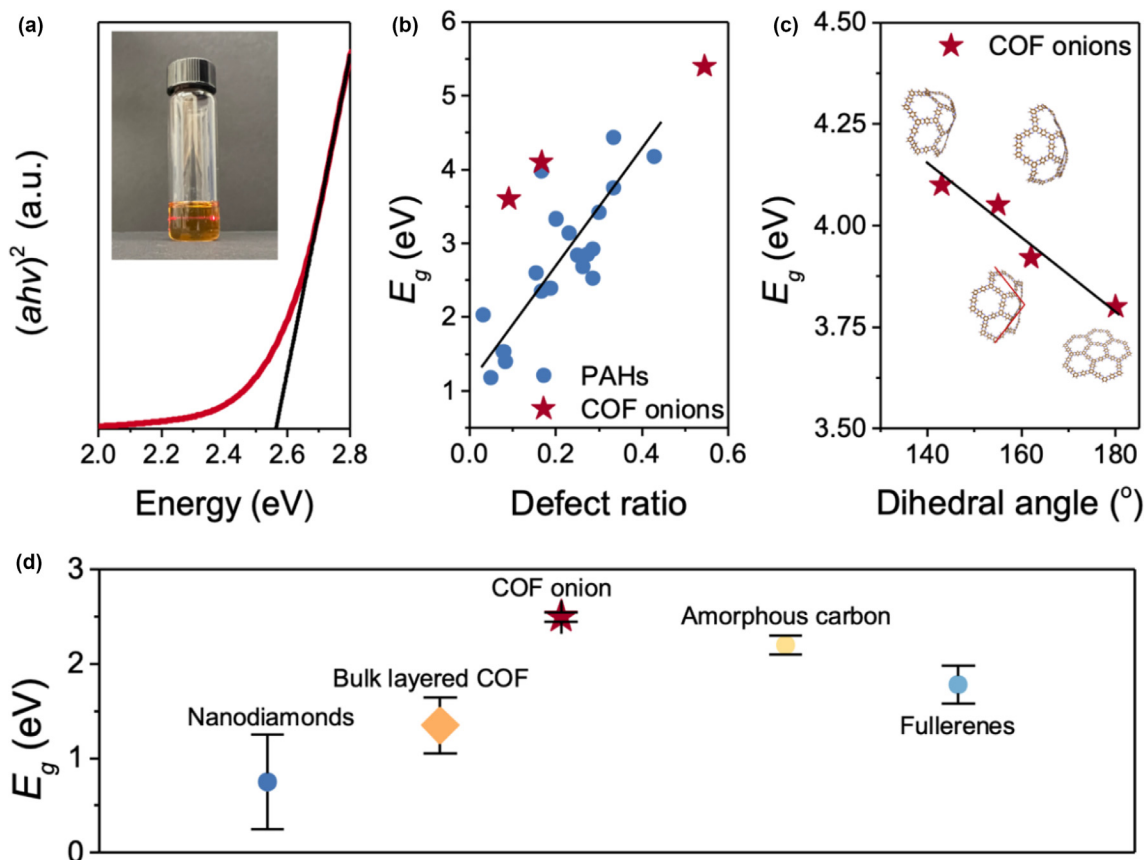


FIGURE 5

Optical properties of COF onions. (a) Tauc plot calculated using an absorption coefficient α and photon energy $h\nu$ (h , Planck constant; ν , frequency) to determine the optical bandgap of COF onions. Extrapolating the linear region (red line) estimates an optical bandgap of 2.5 eV. Inset, the Tyndall effect confirms the colloidal nature of COF onions dispersions. (b, c) Theoretical calculations on how the defects affect the optical bandgap. (b) The relation between defect ratio and the optical bandgap of the COF ion fragments. The defect ratio is defined by the fraction of non-six member rings such as five-, seven-member rings, etc. A similar trend is found in polycyclic aromatic hydrocarbons [47]. (c) The relation between dihedral angle and the value of optical bandgap. Different configurations of the COF fragments are inserted. The dihedral angle is measured within the COF layers. A lower dihedral angle represents a higher curvature of COF layers. (d) Comparison of the bandgap of COF onions against different carbon-based materials, including fullerenes [53], nanodiamonds [54], monolayer amorphous carbon [55], and the bulk COF nanomaterial [27]. The error bar is estimated from multiple measurements.

Conclusions

In summary, we have successfully synthesized a novel COF onion nanostructure through a facile hydrothermal synthesis. This COF onion contains orderly arranged carbon and nitrogen in the aza-fused skeletons, and the size can also be controlled with an average size of 5.7 ± 1.2 nm. The structure of the COF onion is resolved by atomic-resolution TEM imaging and electron energy-loss spectroscopy, which reflects its graphitic layered features and long-range periodicity. Defects, dislocations, and stacking faults are also observed, which account for the formation of such exquisite nanostructures. The COF onion exhibits an optical bandgap similar to other carbon-based nanomaterials, indicating its significant potential in energy storage and catalysis applications. This work reveals insightful information regarding the atomic features of COF onion structures and informs our understanding of their growth mechanisms.

Materials and methods

Preparation of COF onions

1,2,4,5-Benzenetetramine tetrahydrochloride (BTA, 12.8 mg, 0.045 mmol) and hexaketocyclohexane octahydrate (HKH,

9.3 mg, 0.030 mmol) were dissolved in water (2 ml) in a 5 ml-Biotage vial. Note that 45 μ l 4 M potassium hydroxide solution was added as the catalyst. Then, the mixture was degassed by freeze-pump-thaw for three cycles and sealed under vacuum. The vial was heated in an oven at 120 $^\circ$ C for 3 days. Finally, the precipitates were collected by centrifugation, filtration and washed with water and methanol. The precipitates were re-dispersed in N-Methyl-2-Pyrrolidone (NMP) and sonicated for 60 min at 30 $^\circ$ C. To separate the COF onions (\sim 20 nm) from the large bulk samples (\sim μ m), we further centrifuged the dispersion at 10,000 rpm for 10 min (Fig. S8). The supernatant containing COF onions was kept and concentrated. Then the onion sample was drop-casted onto a copper grid (Ultrathin C on lacey, 300 mesh Cu) for further TEM characterization.

Instrumentation

TEM images were acquired using a ThemIS transmission electron microscope with a Thermo Fisher Scientific Ceta CMOS camera. The microscope was operated at 300 keV with the Bruker SuperX energy dispersive X-ray spectroscopy (EDS) detector, allowing rapid chemical identification. Electron energy loss spectroscopy

(EELS) analysis was performed on FEI Tecnai F20 UT at 200 kV in STEM mode with 0.15 eV energy resolution. The energy dispersion was set to 0.3 eV per channel for the full spectrum and 0.02 eV per channel for the near-edge structure of C and N K-edges. Some definitions of the structure parameters and calculation formulas used for Fig. 2 image analysis can be found in Fig. S9. The local interlayer spacing of 2D layers was calculated based on the fast Fourier transform (FFT), using a “rolling window” algorithm through image partition (see more details in Figs. S10–S15). The liquid-state UV–vis absorbance measurement was performed on Cary 5000 UV–vis-NIR spectrometer, from 180 to 1000 nm at the step of 1 nm. Fourier transform infrared (FTIR) spectra were recorded on a Perkin Elmer Spectrum One FTIR system. The solid-state ^{13}C cross-polarization magnetic angle spinning (CP-MAS) NMR spectrum was recorded on the AVANCE II 500 (Bruker, Germany) at a magnetic field strength of 11.7 T.

Theoretical calculations

Optimized geometries of the COF fragments were determined using the 6-311G(d,p) basis set and the B3LYP hybrid functional using the Gaussian package. The theoretical optical bandgap is estimated as the HOMO-LUMO gap determined from the single-point calculation. Molecular dynamics simulations were performed on the LAMMPS platform, using a Verlet algorithm with a time step of 0.1 ps. The ReaxFF force field was chosen [58]. A microcanonical ensemble was employed for 3 ns to relax the structure. All the atomic configurations were visualized in Vesta.

CRedit authorship contribution statement

Qi Zheng: Conceptualization, Methodology, Data curation, Visualization, Writing - original draft, Writing - review & editing. **Xinle Li:** Methodology, Data curation, Writing - original draft. **Qiubo Zhang:** Visualization, Data curation, Investigation, Writing - original draft. **Daewon Lee:** Investigation, Methodology. **Haiyan Mao:** Data curation, Methodology. **Chongqing Yang:** Investigation, Visualization. **Karen C. Bustillo:** Investigation, Methodology. **Jeffrey A. Reimer:** Resources, Supervision. **Yi Liu:** Resources, Supervision. **Haimei Zheng:** Conceptualization, Supervision, Funding acquisition, Investigation, Resources, Writing - original draft, Writing - review & editing.

Declaration of Competing Interest

The authors declare that they have no known competing financial interests or personal relationships that could have appeared to influence the work reported in this paper.

Acknowledgments

This work was supported by the U.S. Department of Energy (DOE), Office of Science, Office of Basic Energy Sciences (BES), Materials Science and Engineering Division under Contract No. DE-AC02-05-CH11231 within the KC22ZH program. J. Jiang acknowledges the support from the National Natural Science Foundation of China (No. 51925903) and the National Key R&D Program of China (2018YFC0705401). D.L. acknowledges the Kwanjeong Study Abroad Scholarship from the KEF (Kwan-

jeong Educational Foundation) (KEF-2019). Work at the Molecular Foundry is supported by the Office of Science, Office of Basic Energy Sciences, of the U.S. Department of Energy under Contract No. DE-AC02-05CH11231.

Appendix A. Supplementary data

Supplementary data to this article can be found online at <https://doi.org/10.1016/j.mattod.2022.09.002>.

References

- [1] B. Trauzettel et al., *Nat. Phys.* 3 (2007) 192–196.
- [2] M. Bacon, S.J. Bradley, T. Nann, *Part. Part. Syst. Charact.* 31 (2014) 415–428.
- [3] H.W. Kroto et al., *Nature* 318 (1985) 162–163.
- [4] W. Krätschmer et al., *Nature* 347 (1990) 354–358.
- [5] K. Kikuchi et al., *Nature* 357 (1992) 142–145.
- [6] Q. Wu et al., *Adv. Mater.* 32 (2020) 1904177.
- [7] A. Aubele et al., *Adv. Mater.* (2021) 2103573.
- [8] R. Tenne, M. Redlich, *Chem. Soc. Rev.* 39 (2010) 1423–1434.
- [9] B. Višić, L.S. Panchakarla, R. Tenne, *J. Am. Chem. Soc.* 139 (2017) 12865–12878.
- [10] A.P. Cote et al., *Science* 310 (2005) 1166–1170.
- [11] N. Huang, P. Wang, D. Jiang, *Nat. Rev. Mater.* 1 (2016) 16068.
- [12] K. Kaiser et al., *Science* 365 (2019) 1299–1301.
- [13] E. Jin et al., *Science* 357 (2017) 673–676.
- [14] L. Zhu et al., *Sci. Adv.* 6 (2020) eaay8361.
- [15] Y.-Y. Liu et al., *Nat. Commun.* 11 (2020) 1–8.
- [16] S. Wan et al., *Angew. Chem. Int. Ed.* 47 (2008) 8826–8830.
- [17] B. Gole et al., *Angew. Chem. Int. Ed.* 57 (2018) 846–850.
- [18] S. Kandambeth et al., *Nat. Commun.* 6 (2015) 1–10.
- [19] H.S. Sasmal et al., *J. Am. Chem. Soc.* 141 (2019) 20371–20379.
- [20] H.S. Sasmal et al., *J. Am. Chem. Soc.* 143 (2021) 8426–8436.
- [21] A. Kumar Mahato et al., *J. Am. Chem. Soc.* 143 (2021) 20916–20926.
- [22] N. Sano et al., *Nature* 414 (2001) 506–507.
- [23] V.V. Pokropivny et al., *J. Solid State Chem.* 154 (2000) 214–222.
- [24] A. Zak et al., *J. Am. Chem. Soc.* 122 (2000) 11108–11116.
- [25] L. Rapoport, N. Fleischer, R. Tenne, *Adv. Mater.* 15 (2003) 651–655.
- [26] A. Albu-Yaron et al., *Adv. Mater.* 18 (2006) 2993–2996.
- [27] X. Li et al., *Chem* 6 (2020) 933–944.
- [28] H.-G. Liao et al., *Science* 345 (2014) 916–919.
- [29] A.S. Barnard, E. Osawa, *Nanoscale* 6 (2014) 1188–1194.
- [30] A.C. Ferrari et al., *Phys. Rev. B* 62 (2000) 11089.
- [31] M. Chhowalla et al., *Phys. Rev. Lett.* 90 (2003) 155504.
- [32] P. Wesolowski et al., *Appl. Phys. Lett.* 71 (1997) 1948–1950.
- [33] O. Stephan et al., *Science* 266 (1994) 1683–1685.
- [34] S. Waidmann et al., *Diam. Relat. Mater.* 9 (2000) 722–727.
- [35] M. Terrones, N. Grobert, H. Terrones, *Carbon N. Y.* 40 (2002) 1665–1684.
- [36] L. Laffont et al., *Carbon N. Y.* 42 (2004) 2485–2494.
- [37] C.Y. Zhang, J.M. Tour, *J. Am. Chem. Soc.* 121 (1999) 8783–8790.
- [38] Z. Xu et al., *Adv. Mater.* 28 (2016) 1981–1987.
- [39] M. Karplus, J.A. Pople, *J. Chem. Phys.* 38 (1963) 2803–2807.
- [40] B.T. Koo, W.R. Dichtel, P. Clancy, *J. Mater. Chem.* 22 (2012) 17460–17469.
- [41] B.H. Kim et al., *Science* 368 (2020) 60–67.
- [42] C.-C. Chen et al., *Nature* 496 (2013) 74–77.
- [43] N.D. Loh et al., *Nat. Chem.* 9 (2017) 77–82.
- [44] H. Terrones, M. Terrones, *J. Phys. Chem. Solids* 58 (1997) 1789–1796.
- [45] A. Chuvilin et al., *Nat. Chem.* 2 (2010) 450–453.
- [46] C. Jäger et al., *Astrophys. J.* 696 (2009) 706.
- [47] A. Menon et al., *Phys. Chem. Chem. Phys.* 21 (2019) 16240–16251.
- [48] Y.-W. Son, M.L. Cohen, S.G. Louie, *Phys. Rev. Lett.* 97 (2006) 216803.
- [49] M. Topsakal et al., *Phys. Rev. B* 78 (2008) 235435.
- [50] J. Cai et al., *Nature* 466 (2010) 470–473.
- [51] M.D. Diener, J.M. Alford, *Nature* 393 (1998) 668–671.
- [52] N. Lou, Y. Li, L. Gan, *Angew. Chemie Int. Ed.* 56 (2017) 2403–2407.
- [53] R. Pincak et al., *Fullerenes Nanotub. Carbon Nanostruct.* 25 (2017) 607–612.
- [54] I.I. Vlasov et al., *Nat. Nanotechnol.* 9 (2014) 54–58.
- [55] C.-T. Toh et al., *Nature* 577 (2020) 199–203.
- [56] Q. Huang et al., *Nature* 510 (2014) 250–253.
- [57] T. Cheng et al., *Adv. Mater.* 27 (2015) 3349–3376.
- [58] A.M. Kamat, A.C.T. Van Duin, A. Yakovlev, *J. Phys. Chem. A* 114 (2010) 12561–12572.